Short-time Coherent Incoherent Synthetic Aperture Radar Processing for a Handheld Imaging System

Guillermo Álvarez-Narciandi, *Member, IEEE*, Jaime Laviada, and Fernando Las-Heras, *Senior Member, IEEE*

***Abstract*—This paper presents a processing technique that mitigates the impact of positioning errors on the quality of the images retrieved using handheld (or portable) scanners based on synthetic aperture radar (SAR). These systems rely on the use of tracking systems to combine the information acquired at multiple positions to achieve high-resolution images. This is specially challenging at millimeter-wave (mmWave) frequencies in the absence of high-accuracy tracking systems external to the handheld scanner. To this end, the proposed technique employs a hybrid coherent-incoherent SAR processing method especially suited for mitigating the impact of positioning errors from tracking systems performing simultaneous localization and mapping (SLAM).**

The proposed technique was experimentally validated using a handheld scanner comprising a compact radar module and a tracking camera that performs SLAM. Results show that if a fully-coherent processing is used, the quality of the obtained images is greatly degraded, and if a fully-incoherent processing is considered, there is a significant resolution loss, which prevents from accurately imaging the shape of the targets. In contrast, using the presented method it is possible to successfully image the targets, mitigating the impact of positioning errors from the tracking camera.

***Index Terms*—MmWave imaging; freehand; synthetic aperture radar; handheld system; coherent processing; incoherent processing; portable system.**

I. Introduction

ELECTROMAGNETIC imaging is an enabling technology for multiple applications ranging from security screening [1], [2], [3], [4] and landmine detection [5], to non-destructive evaluation [6], [7], [8], [9] and medical diagnosis [10], [11], to name a few. In particular, it relies on the capability of electromagnetic waves to penetrate through certain optically opaque materials [12], enabling the inspection of areas which cannot be assessed using the visible spectrum. Electromagnetic imaging systems can be found under different implementations. One example are the booth-size systems that are deployed at many airports for people screening. These systems provide high-resolution images and a fast acquisition speed relying on large apertures generated using a significant amount of transmitters (Tx) and receivers (Rx), doing a raster scan with a reduced number of them, or resorting to multiple-input multiple-output configurations [2]. However, in some applications the use of such large and complex systems is not feasible nor practical, which has encouraged the development of portable and compact alternatives. Towards this goal, a microwave camera was developed in [13], [14]. An analogous system at the millimeter-wave (mmWave) band was presented in [15]. Both systems employ a medium-size physical aperture ($\approx 20-30\,\text{cm}$) operating at close range offering a good trade-off between size and resolution. Moreover, these systems can benefit from multiview techniques to increase their field of view [16]. A different approach presented in [17], [18] leverages the advances in mmWave technology, which have enabled the development of radar-on-chip modules of significantly reduced size [19], [20], [21]. This method, denoted as *freehand imaging*, is based on moving a compact radar module by hand taking measurements of the area under inspection while its position is tracked by a positioning system. The acquisitions from different positions are coherently combined by means of a synthetic aperture radar (SAR) algorithm, which enables to obtain high-resolution images of the scene bypassing the need of a large physical aperture, and without resorting to a bulky positioning system. In particular, the images of the area under investigation can be updated as measurements are acquired, conferring great flexibility to the operator of the system, which can dynamically decide where to take measurements or if enough information has been acquired with the handheld scanner.

One of the challenges faced by this kind of systems is that the measurements are not acquired uniformly, which prevents the straightforward use of highly efficient algorithms based on fast Fourier Transforms [22]. This is a constraint also inherent to other vehicle or UAV mounted [5] systems, and a significant research effort has been devoted to develop efficient algorithms to process this kind of data [23], [24], [25], [26]. Moreover, the inspected area might be sparsely sampled, specially at the beginning of the scanning process, causing undesired artifacts in the reflectivity images of the scene. In this regard, the use of deep-learning techniques, such as vision transformers [27] or conditional generative adversarial networks (cGANs) [28], [29], [30], [31], has been explored to improve the quality of the obtained images.

Another issue that has a major impact on the quality of the retrieved images is the tracking accuracy of the handheld scanner [32], [33]. As previously explained, freehand imaging systems rely on a positioning system to combine measurements acquired at different positions. This enables the use of SAR processing techniques to overcome the limited

This work has been partially supported by Project PID2021-122697OB-I00 funded by MCIN/ AEI / 10.13039/501100011033 / FEDER, UE; by the UKRI Postdoctoral Fellowship Guarantee for MSCA PF under Project EP/X022943/1; and by Gobierno del Principado de Asturias/FEDER under grant AYUD/2021/51706. The data that support the findings of this study are available upon reasonable request.

Guillermo Álvarez-Narciandi is with the Centre for Wireless Innovation, Queen's University Belfast, United Kingdom (e-mail: g.alvarez-narciandi@qub.ac.uk). Jaime Laviada and Fernando Las-Heras are with the Department of Electrical Engineering, University of Oviedo, Spain.

resolution that can be obtained with a standalone acquisition of a compact radar module. Thus, the positioning accuracy of the considered localization system can severely affect the quality of the images obtained with these systems, specially at mmWave frequencies, where even small tracking errors are significant in terms of electrical size. In this regard, the use of laser trackers or motion capture systems, which were considered both for freehand imaging [17], [18] and freehand antenna measurement [34], [35] systems, provide enough accuracy to coherently combine measurements acquired with a handheld scanner. However, the capability to embed the tracking system in the handheld scanner would be of great interest. Some of the current 5G devices comprise mmWave modules and this trend is expected to grow towards 6G, where joint communications and sensing is expected to play a major role [36], [37]. This kind of general purpose handheld devices (e.g., smartphones) have multiple sensors, such as cameras and inertial measurement units (IMUs), that can be leveraged to enable simultaneous localization and mapping (SLAM). These features make these devices ideal to develop freehand imaging scanners, enabling a wide-range of applications. SLAM algorithms aim at estimating the trajectory of the sensor while mapping its surrounding environment. A feasibility study of employing a tracking camera performing SLAM for a freehand imaging system was presented in [38]. Although this approach provides enough accuracy to perform imaging, it is not as good as the one obtained with other methods such as motion capture systems, which has an impact on the quality of the obtained images. Moreover, SLAM systems might drift over time until they re-localize [39]. Therefore, it is necessary to develop processing techniques that mitigate the impact of these positioning errors on the imaging performance of the scanner.

This work presents a hybrid coherent-incoherent SAR processing that limits the impact of positioning errors of tracking systems, and more specifically, SLAM systems, on the quality of the electromagnetic images obtained with a mmWave freehand scanner. The proposed method is experimentally validated using a handheld scanner prototype comprising a mmWave radar module and a tracking camera, showing its capability to mitigate the effect of positioning errors in the quality of the images produced by a handheld scanner.

This paper is organized as follows. First, the considered system is presented in Section II, where the proposed technique is explained. Then, the impact of the presented method is experimentally assessed in Section III, and finally the conclusions are drawn in Section IV.

II. Description of the System

In this Section, the architecture of the system is presented and the proposed imaging algorithm is discussed.

A. Architecture

As previously explained, freehand imaging systems are based on the use of a compact size radar module, which can be easily handled by hand, that is moved over the area under inspection taking measurements while its position is being tracked. Therefore, the information from the different acquisitions can be coherently combined to produce a high-resolution radar image. In this case, the freehand scanner comprises a frequency-stepped continuous-wave radar-on-chip module with 20 transmitters and 20 receivers [21], yielding a total of 400 independent radiofrequency channels. The Tx are equally spaced along a line of $40\,$mm. In a similar fashion, the Rx are distributed along a line of $41.6\,$mm, orthogonal and with an offset with respect to the Tx array, yielding a physical aperture of $55\,\text{mm} \times 53.4\,\text{mm}$. This module, whose main parameters are summarized in Table I, was used in preliminary studies for freehand imaging in [40], [41]. During its operation, the transmitters are activated sequentially and the receivers work concurrently. The radar frequency bandwidth is $7\,$GHz (from $62\,$GHz to $69\,$GHz), resulting in a range resolution of $\delta_z \approx 4.3\,$cm, and its size is $8\,\text{cm} \times 8\,\text{cm}$. The positioning system used to track the movement of the radar module is a lightweight and compact stereoscopic tracking camera including two fisheye lens sensors and an IMU [42] capable of performing SLAM. Therefore, both the radar module and the tracking system are assembled in the handheld scanner, which is depicted in Fig. 1, by means of a 3D-printed structure. The reflective markers that can be observed in Fig. 1(b) were included as part of the high-accuracy motion capture system [43] based on the use of infrared cameras that was used as a reference tracking system during the validation of the proposed handheld scanner and processing technique. The radar module and the tracking camera are controlled from a conventional laptop which triggers synchronized acquisitions from both devices, processes the obtained information, and displays the retrieved electromagnetic image of the area under investigation, which is updated as more measurements are performed. The laptop was equipped with 32 GB of RAM, a processor Intel i7-10875H at $2.3\,$GHz and a NVIDIA GeForce RTX2060.

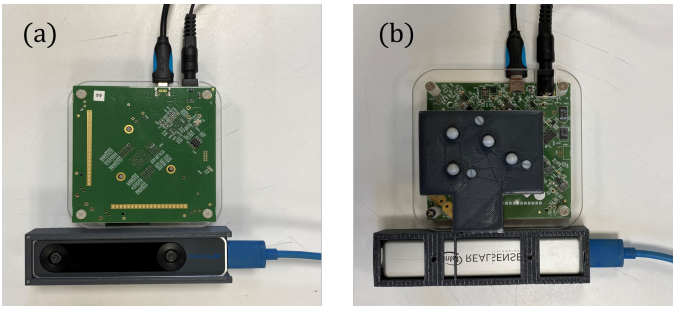

Fig. 1. (a) Top and (b) bottom view of the freehand imager.

Table I
Main parameters of the radar module.

# of Tx	# of Rx	Bandwidth	δ_z	Resolution bandwidth	Frequency points	Physical aperture
20	20	7 GHz	4.3 cm	30 kHz	128	55 mm×53.4 mm

B. Imaging algorithm

A freehand imaging system entails some constraints that limit the processing techniques that can be considered. First, as previously introduced, due to their handheld nature, the acquired measurements will not be uniformly distributed nor sampled according to a specific acquisition pattern. Instead, the acquisition positions will be irregularly distributed across the observation domain. Second, it is desired to display real-time results to the operator of the handheld imager, so that it is possible to switch the focus of the scan on a given area, or to decide if enough information has been acquired. These constraints prevent the use of highly efficient algorithms based on fast Fourier Transforms operations, which are usually developed for regular acquisitions [22]. Instead, it is possible to resort to a delay-and-sum algorithm to coherently combine the acquired measurements (i.e., complex summation after a phase compensation term is applied). This enables to process nonuniformly acquired samples and direct updates of the reflectivity of the area under investigation as more measurements are acquired. In that case, the reflectivity, ρ, at the different points, $\mathbf{r}'$, in which the investigation domain, i.e., the area under investigation, is discretized, after the m-th acquisition of the radar module is given by

$$\rho_m(\mathbf{r}')=\sum_{i=1}^{m}\sum_{p=1}^{N_{RX}}\sum_{n=1}^{N_{TX}}\sum_{q=1}^{N_{freq}} S_{i,p,n}(\mathbf{r},f_q)e^{j\frac{2\pi f_q}{c}(R_{Tx}+R_{Rx})}, \quad (1)$$

where S refers to the complex baseband signal, f denotes the frequency, and c the speed of light. N_{TX} and N_{RX} are the number of transmitters and receivers of the radar module, respectively, and N_{freq} is the number of frequency points of the radar signal, S. The terms R_{Tx} and R_{Rx} are given by

$$\begin{aligned} R_{Tx} &= ||\mathbf{r}' - \mathbf{r_{tx,n}}|| \\ R_{Rx} &= ||\mathbf{r}' - \mathbf{r_{rx,p}}|| \end{aligned}, \quad (2)$$

where $\mathbf{r_{tx,n}}$ and $\mathbf{r_{rx,p}}$ are the position of the n-th transmitter and that of the p-th receiver of the radar module at the m-th acquisition position. It should be remarked that the calculation of (1) is spread along the entire acquisition, i.e., the reflectivity is updated after each new sample is measured. Thus, a final computationally-intensive operation is avoided, and real-time results are displayed to the operator of the scanner. Alternatively, optimized approaches have also been recently proposed for irregular data [23].

As previously introduced, the coherent combination of radar measurements is greatly affected by positioning errors, especially in the vertical direction [44]. In particular, this is significantly demanding in terms of accuracy for tracking systems when mmWave frequencies are considered. In contrast, the incoherent combination of measurements is less sensitive to positioning errors, at the expense of a reduced resolution. In this paper, we propose a short-time coherent-incoherent approach to mitigate the impact of positioning errors on the quality of electromagnetic images while reducing the resolution loss if a fully-incoherent processing is adopted. In particular, Eq. (1) is modified to perform an incoherent combination after a set of M new measurements are acquired:

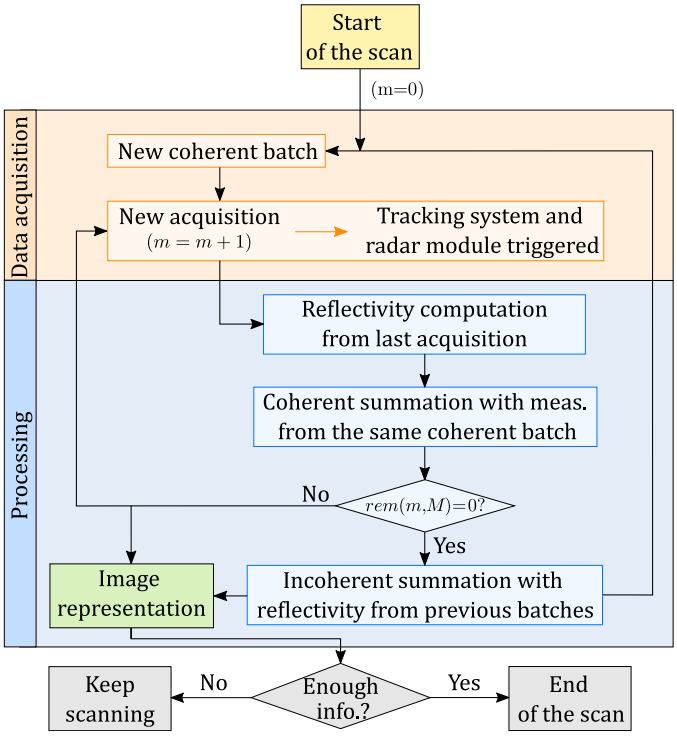

Fig. 2. Flow diagram of a freehand scan following the presented technique, where $rem(m, M)$ denotes the remainder of dividing m by M.

$$\rho_m(\mathbf{r}')=\sum_{l=1}^{\lfloor \frac{m}{M} \rfloor}\left|\sum_{\substack{i=1+\\(l-1)M,\\ i<=m}}^{lM}\sum_{p,n,q} S_{i,p,n}(\mathbf{r},f_q)e^{j\frac{2\pi f_q(R_{Tx}+R_{Rx})}{c}}\right|, \quad (3)$$

where the limits of the inner summations (indexes p, n, and q) have been dropped for conciseness, but remain the same as in Eq. (1). If $M = m$, then a coherent processing is performed, and therefore the impact of positioning errors will be higher. In contrast, if $M = 1$ the measurements are processed in a fully-incoherent manner (i.e., by means of a scalar summation). The workflow of a freehand scan using the proposed technique is summarized in Fig. 2. The reflectivity of the scene is computed using the data of each standalone acquisition of the radar module (inner summation of (3)), and it is coherently combined with that obtained from the other acquisitions of the same coherent batch (second summation of (3)). That is, the information from a total of M different acquisitions is combined when the coherent batch is complete. Every time a new batch is completed, the reflectivity computed from the M acquisitions that are part of the batch is summed incoherently to the reflectivity obtained from previous batches. This scalar combination (i.e., neglecting the phase information) between different coherent batches is denoted by the outer summation of (3). It should be remarked that the scanning process continues until the operator of the scanner, which sees the updated reflectivity image as more measurements are acquired, considers that enough information has been acquired.

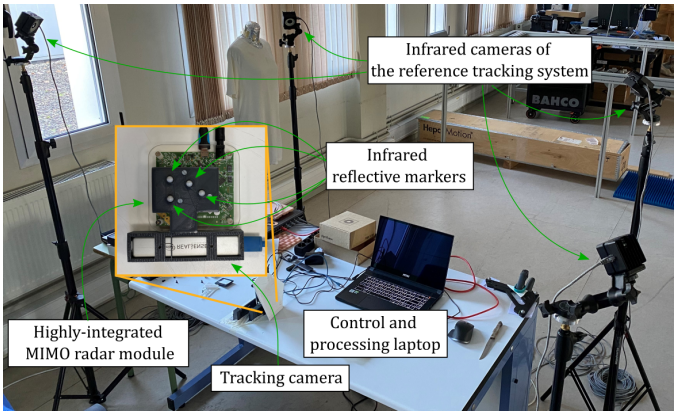

Fig. 3. Image of the measurement setup.

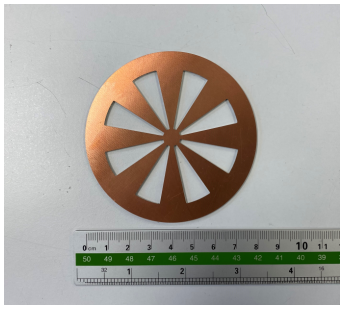

Fig. 4. Image of the star test target.

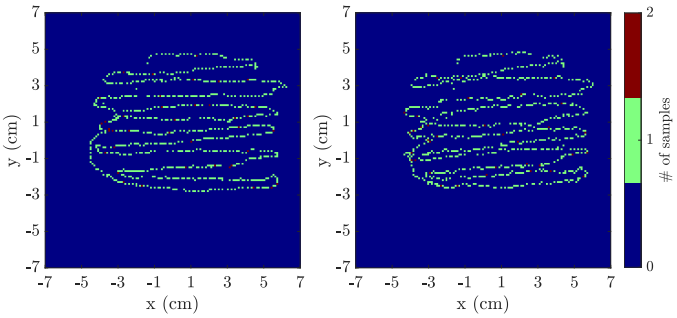

Fig. 5. Heatmap for the star test target showing the positions where radar acquisitions were performed from (a) the reference motion capture system tracking, and (b) the tracking camera of the handheld scanner.

During the experimental validation of the proposed approach, not only is demonstrated that the short-time coherent incoherent processing helps to mitigate the image artifacts generated by tracking errors, but also that the value of M can be tuned to find a trade-off between the resolution loss derived from the incoherent processing and the artifacts due to tracking errors, which depend on the accuracy of the tracking system used in the scanner.

III. Experimental Validation

The performance of the proposed hybrid short-time coherent incoherent processing to mitigate the impact of positioning errors on the quality of images generated with handheld (or portable) scanners was experimentally assessed. For that purpose, several tests with the scanner presented in Section II-A and considering different test targets were performed. In addition, a reference motion capture system, which comprises four infrared cameras (deployed and calibrated at the laboratory where the tests took place), and four reflective markers attached to the handheld scanner (as shown in Fig. 1(b)), was used to obtain a ground-truth position estimation of the scanner. This motion capture system offers sub-mm accuracy [43] and has been successfully used in the context of mmWave imaging [17], [18] and mmWave antenna diagnosis and characterization [34], [35]. The measurement setup, including the cameras of the reference motion capture system, is depicted in Fig. 3.

For the first test, the star test target shown in Fig. 4 was considered. The star has a radius of $4\,$cm and 8 spokes uniformly distributed. During the scan a total of 802 acquisitions were performed during $218\,$s at an average distance of $5.7\,$cm from the target. The distribution of the positions of the acquired measurements obtained with the reference motion capture system and with the tracking camera of the handheld scanner are shown in Fig. 5a and Fig. 5b, respectively. As it can be seen, the handheld scanner was moved over the area of interest describing a *zig-zag* trajectory. Furthermore, due to the handheld nature of the scan, the samples are not uniformly distributed.

The obtained results are shown in Fig. 6. The images of the upper row (Figs. 6a-6e) were obtained considering the tracking information from the reference motion capture system, whilst those in the bottom row (Figs. 6f-6j) were retrieved considering the information from the tracking camera embedded in the handheld scanner. A coherent combination of all the acquired measurements was considered to retrieve Fig. 6a and Fig. 6f. As it can be observed, in Fig. 6a, obtained using the reference motion capture system, the shape of the star target, including all the spokes, is well reconstructed, and the clutter level is low. In contrast, when the information from the tracking camera is used to combine the measurements, Fig. 6f, the shape of the target cannot be recovered, specially the inner parts of the star, and a significant number of artifacts appears in the retrieved image. This is due to the lower accuracy of the tracking camera embedded in the handheld scanner which, as previously explained, performs SLAM, which in turn causes it to sometimes drift until the camera is able to re-localize itself [39]. Figs. 6b-6e and Figs. 6g-6j were computed considering the proposed method for different values of M (i.e., the number of measurements after an incoherent combination is performed) using the positioning information from the reference motion capture system, and from the tracking camera of the handheld scanner, respectively. When $M = 100$ and the motion capture system is used, Fig. 6b, as in the case of a fully-coherent combination of the measurements, the shape of the target is well-reconstructed. However, although the quality of the image is still high, the clutter level increases, and the resolution is slightly reduced, which can be noticed in the spokes of the star. In the case of considering the positioning information from the tracking camera, there is a

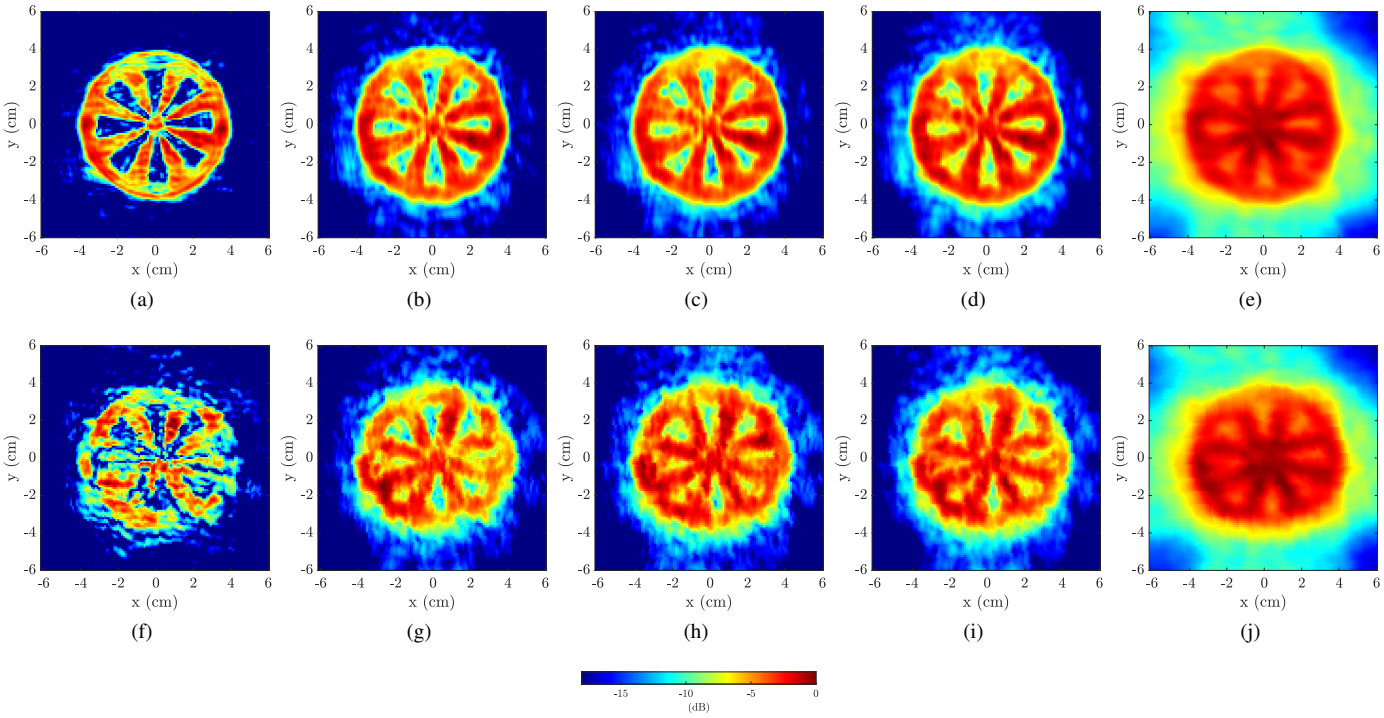

Fig. 6. Images of the star test target obtained considering the reference motion capture system and (a) performing a fully-coherent combination of the measurements, and using the proposed technique for (b) $M = 100$, (c) $M = 85$, (d) $M = 50$, and (e) $M = 1$ (i.e., fully-incoherent combination). The same when the tracking camera is used: (f) fully-coherent combination, and the proposed technique for (g) $M = 100$, (h) $M = 85$, (i) $M = 50$, and (j) $M = 1$.

clear improvement on the quality of the image of the target when, instead of considering a fully-coherent combination of the measurements (Fig. 6f), the proposed technique for $M = 100$ is used (Fig. 6g). In particular, in the former case (Fig. 6f) the shape of the target cannot be distinguished and there is a high number of artifacts in the image. In contrast, when the proposed technique for $M = 100$ is considered (Fig. 6g) the shape of the target is imaged and their main features can be reconstructed. Although the obtained image exhibits a lower quality than Fig. 6b, obtained with the motion capture system, it is still sufficient to identify the target and its main characteristics. Therefore, the proposed technique mitigates the impact of the positioning errors of the tracking camera, enabling the use of a handheld scanner that does not rely on external infrastructure to produce high-resolution images.

Figs. 6c and 6h were retrieved using the proposed technique and $M = 85$, relying on the data from the reference motion capture system, and that from the tracking camera, respectively. Fig. 6c shows a similar quality as 6b, obtained for $M = 100$. In contrast, in Fig. 6h the shape of the target resembles the true one of the target slightly better than in Fig. 6g (in particular, the outer perimeter and the left side spokes), although the clutter level is higher. When $M = 50$ (Figs. 6d and 6i using the reference motion capture system and the tracking camera, respectively) the shape of the target is still well-reconstructed, although the resolution worsens marginally and the clutter level increases. Finally, when $M = 1$, i.e., a fully incoherent combination of the measurements, the resolution of the retrieved images is drastically reduced, as can be observed in Figs. 6e and 6j, which were computed

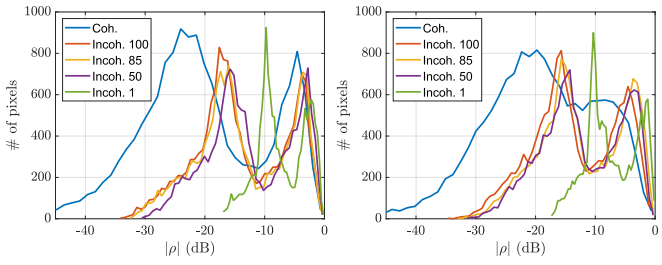

Fig. 7. Histogram of the normalized reflectivity value of the pixels of the retrieved images using (a) the reference motion capture system tracking, and (b) the tracking camera of the handheld scanner.

using the data from the reference motion capture system and the tracking camera, respectively. These results show that the proposed technique can be used to mitigate the impact of the positioning errors of the tracking camera, enabling to obtain good quality images of targets without the resolution loss that occurs when a fully-incoherent combination of the measurements is considered. Regarding the value of M, the three intermediate values considered (100, 85, and 50) yield good quality images. In addition, while lower values of M do not result in an image quality improvement, the resolution progressively decreases until the case of $M = 1$, i.e., a fully incoherent combination of the measurements.

To complement the previous discussion, Fig. 7 shows the histograms of the normalized reflectivity value of the pixels of the different images of Fig. 6. In particular, the histograms of the images computed using the positioning information from

Table II
MS-SSIM INDEX OF THE IMAGES OF THE STAR TEST TARGET DEPICTED IN FIG. 6

	Processing method				
Positioning system	Fully-coherent	$M = 100$	$M = 85$	$M = 50$	Fully-incoherent
Motion capture system	0.89	0.85	0.81	0.74	0.28
Tracking camera	0.53	0.69	0.69	0.68	0.29

Fig. 8. Image of the letters used as test target.

the reference motion capture system are displayed in Fig. 7a. As it can be seen, in Fig. 7a in every case (fully-coherent combination, using the proposed technique and $M = 100$, $M = 85$, and $M = 50$, and fully-incoherent combination), there are two prominent peaks: one around the reflectivity value of the pixels corresponding to the target, and a second one (the lowest) around the clutter level of the image. The greatest reflectivity level difference between these peaks takes place when a fully-coherent combination is considered, indicating that the contrast between the target and the clutter is higher. This difference is reduced when the proposed technique and $M = 100$, $M = 85$, and $M = 50$ are considered, but it is still around 15 dB. However, it is significantly reduced when measurements are combined incoherently, in agreement with the previous discussion. The histograms of the images retrieved using the positioning information from the tracking camera of the handheld scanner are displayed in Fig. 7b. In this case, when a fully-coherent combination is performed the two peaks cannot be distinguished. This is due to the significant number of artifacts that appear in the image, where the shape of the target cannot be reconstructed. In contrast, when the proposed technique is applied, the histograms of the images follow a similar pattern as when the positioning information from the reference motion capture system is used.

Finally, in order to quantitatively compare the images, their multi-scale structural similarity (MS-SSIM) index [45] was computed to compare them with a reference image with the exact size and shape of the target. The MS-SSIM metric extracts the structural information from the scene, providing a good approximation of the perceived image quality. MS-SSIM values closer to 1 denote better image quality, whilst values closer to 0 mean worse image quality. The results are summarized in Table II. As expected, the best image quality

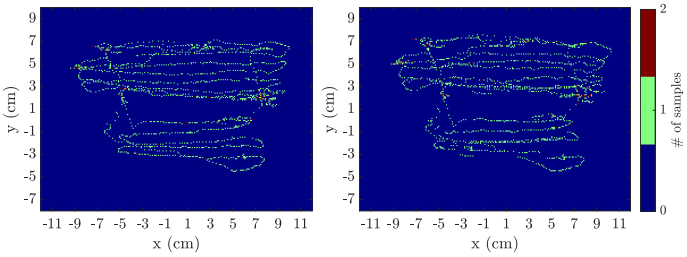

Fig. 9. Heatmap for the letters test target showing the positions where radar acquisitions were performed from (a) the reference motion capture system tracking, and (b) the tracking camera of the handheld scanner.

is achieved when the reference motion capture system is used and, more specifically, when a fully-coherent combination of the measurements is applied. When the tracking camera is used and a fully-coherent combination is considered, the MS-SSIM index is low, denoting a poor image quality. However, when the proposed technique is applied (for $M = 100$, $M = 85$, and $M = 50$), the MS-SSIM index increases notably, i.e., the quality of the images improves significantly, in agreement with the previous discussion from a qualitative point of view. Finally, when a fully-incoherent processing is applied, using either the positioning information from the reference motion capture system or from the tracking camera of the handheld scanner, the MS-SSIM index decreases drastically.

A second test was performed with the target shown in Fig. 8. In this case the target was formed by the letters of the acronym of the research group from the University of Oviedo: *TSC-UO*. The target occupies an area slightly over 17 cm × 11 cm. During the scan a total of 1533 measurements were acquired during 468 s at an average distance of 5.9 cm from the target. The distribution of the positions where acquisitions were performed using the information from the reference motion capture system is depicted in Fig. 9a, and in Fig. 9b when the data from the tracking camera is considered.

The obtained results are shown in Fig. 10. In a similar fashion to the results for the previous test target, the set of images computed using the positioning information from the reference motion capture system is displayed on the first row (Figs. 10a-10e). The images retrieved using the data from the tracking camera embedded in the handheld scanner are shown in the bottom row (Figs. 10f-10j). Fig. 10a and Fig. 10f were computed coherently combining all the acquired measurements. As it can be observed, when the motion capture system is used, although the upper right part of the "T" has a lower reflectivity level, the shape of the letters is accurately reconstructed and the clutter level is low. However, if the tracking camera is used to combine the measurements, the coherence is severely degraded, preventing the targets from being recognized. Figs. 10b-10d and Figs. 10g-10i show the images computed using the proposed technique for $M = 100$, $M = 85$, and $M = 50$ using the positioning information from the reference motion capture system and from the tracking camera of the handheld scanner, respectively. In the former case, as when a fully-coherent combination of the measurements is performed, the

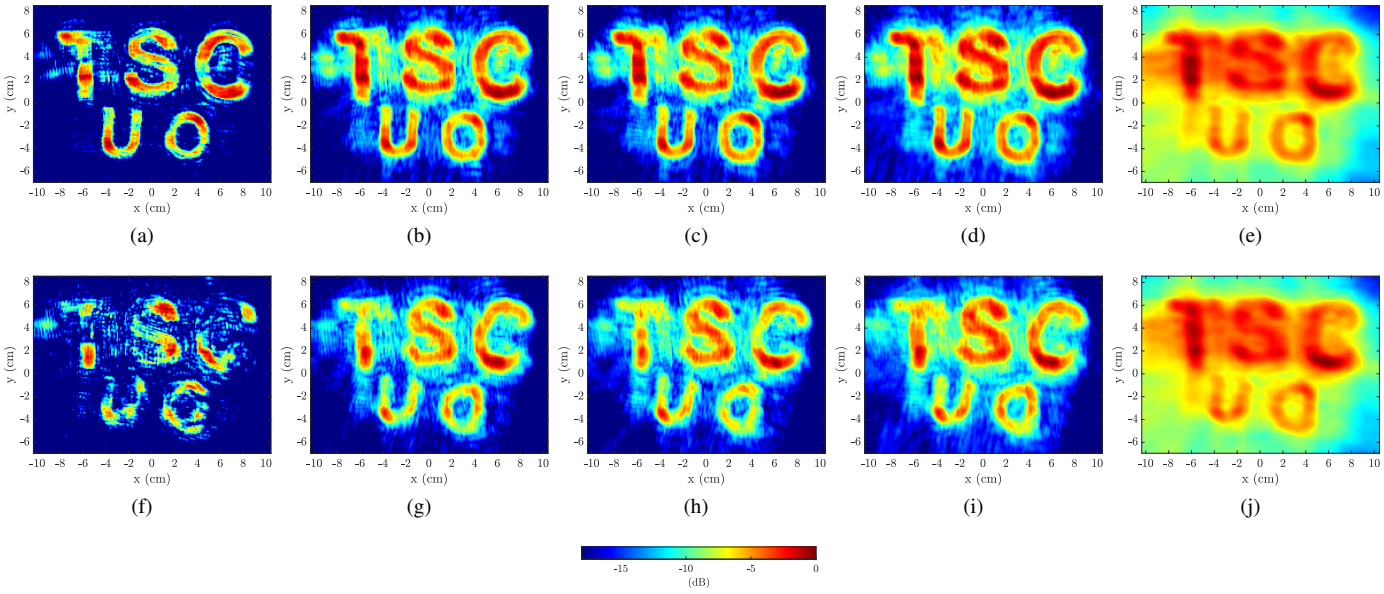

Fig. 10. Images of the letters used as test target obtained considering the reference motion capture system and (a) performing a fully-coherent combination of the measurements, and using the proposed technique for (b) $M = 100$, (c) $M = 85$, (d) $M = 50$, and (e) $M = 1$ (i.e., fully-incoherent combination). The same when the tracking camera is used: (f) fully-coherent combination, and the proposed technique for (g) $M = 100$, (h) $M = 85$, (i) $M = 50$, and (j) $M = 1$.

Table III
MS-SSIM INDEX OF THE IMAGES OF THE LETTERS USED AS TEST TARGET DEPICTED IN FIG. 10

	Processing method				
Positioning system	Fully-coherent	$M = 100$	$M = 85$	$M = 50$	Fully-incoherent
Motion capture system	0.80	0.82	0.82	0.74	0.26
Tracking camera	0.46	0.75	0.76	0.75	0.25

quality of the obtained images is high as the shape of the targets can be clearly distinguished above the clutter level, which increases as the value of M is reduced. In the latter case, i.e., when the positioning information from the tracking camera is used to combine the acquired measurements, the use of the proposed technique improves significantly the quality of the retrieved images in comparison to the case of a fully-coherent processing. In particular, although the background clutter level of the obtained images is higher, the shape of the targets is well-reconstructed, whilst in the case of the fully-coherent processing the letters could not be recognized. Finally, the images displayed in Fig. 10e and Fig. 10j were retrieved performing a fully-incoherent combination of the measurements (i.e., $M = 1$) using the positioning information from the motion capture system and that from the tracking camera of the handheld scanner, respectively. As it can be seen, the quality of both images is very poor, as there is a significant resolution loss and an important clutter level increment.

In order to quantitatively compare the obtained results, the MS-SSIM index of the retrieved images was computed using a reference image with the exact size and shape of the letters used as targets. The MS-SSIM values are summarized in Table III. As it was expected, the highest value of the MS-SSIM index is obtained when the reference motion capture system is used. When a fully-coherent combination is performed employing the positioning data from the tracking camera the MS-SSIM index is low, indicating a poor image quality. This also confirms the previous discussion from a qualitative point of view, as the shape of the targets was not recognizable in Fig. 10f. If the proposed technique for $M = 100$, $M = 85$, and $M = 50$ is used to process the measurements, the values of the MS-SSIM index increase significantly, being comparable to the MS-SSIM index value obtained using the reference motion capture system and the proposed technique for $M = 50$. This shows that the proposed technique can be successfully used to mitigate the positioning errors of the tracking camera, enabling to retrieve high-resolution images without the need of an external positioning system. Finally, when all measurements are combined incoherently, the MS-SSIM index decreases drastically using both positioning systems, confirming that resorting to this type of processing results in a severely worsened image quality.

IV. CONCLUSIONS

This manuscript presents a technique to mitigate the impact of positioning errors on the quality of the images produced by handheld (or portable) scanners, while limiting the resolution loss when an incoherent processing is performed. This is of special interest due to the growth in the number of systems and devices using mmWave radiofrequency modules, which also frequently include other sensors that can be leveraged for localization purposes and SLAM. Thus, if the impact of tracking errors can be reduced, these devices could be turned into mmWave scanners without resorting to external infrastructure, enabling multiple applications. The proposed approach

is based on a hybrid coherent-incoherent SAR processing that enables the use of nonuniformly acquired data, as is the case of most radar systems mounted on vehicles or moved by hand, and regular updates of the estimated reflectivity of the scene as more measurements are gathered. In particular, the acquired measurements are coherently combined until M samples are obtained, when they are summed incoherently to the reflectivity of the scene under investigation. Moreover, the value of M can be tuned to reduce the resolution loss resulting from the incoherent processing depending on the accuracy of the tracking system used in the scanner.

The proposed technique was experimentally validated processing the measurements acquired with a handheld scanner comprising a compact radar module and a tracking camera capable of performing SLAM. In addition, a external high-accuracy motion capture system was also used to obtain a reference measurement of the positioning information of the handheld scanner during the scans. Two set of targets were scanned with the prototype, and the reflectivity images of the scene considering a fully-coherent combination of the measurements, a fully-incoherent processing, and the proposed technique for different values of M, were computed using the positioning information from both the high-accuracy reference motion capture system and from the tracking camera embedded in the handheld scanner. Results show that, as expected, when the motion capture system is used to coherently combine the measurements, the quality of the obtained images is significantly high. However, if instead the data from the tracking camera is considered, the quality of the images decrease notably, as a great number of artifacts appear and it is no longer possible to reconstruct the shape of the targets. In contrast, it has been shown that, when the proposed technique is used to process the measurements, it is possible to successfully image the targets employing the positioning information from the tracking camera, at the expense of a higher background clutter level. However, unlike when a fully-incoherent combination of the measurements is performed, the images still present enough resolution to identify the shape of the targets of the scene under investigation, paving the way to the development of completely standalone mmWave scanners.

REFERENCES

[1] D. M. Sheen, D. L. McMakin, and T. E. Hall, "Three-dimensional millimeter-wave imaging for concealed weapon detection," *IEEE Trans. Microw. Theory Tech.*, vol. 49, no. 9, pp. 1581–1592, Sep. 2001.

[2] S. S. Ahmed, A. Schiessl, and L. P. Schmidt, "A novel fully electronic active real-time imager based on a planar multistatic sparse array," *IEEE Trans. Microw. Theory Techn.*, vol. 59, no. 12, pp. 3567–3576, Dec 2011.

[3] J. N. Gollub, O. Yurduseven, K. P. Trofatter, D. Arnitz, M. F. Imani, T. Sleasman, M. Boyarsky, A. Rose, A. Pedross-Engel, H. Odabasi, T. Zvolensky, G. Lipworth, D. Brandy, D. L. Marks, M. S. Reynolds, and D. R. Smith, "Large metasurface aperture for millimeter wave computational imaging at the human-scale," *Scientific Reports*, vol. 20, pp. 1–9, Feb 2017.

[4] Z. Wang, T. Chang, and H.-L. Cui, "Review of Active Millimeter Wave Imaging Techniques for Personnel Security Screening," *IEEE Access*, vol. 7, pp. 148 336–148 350, 2019.

[5] M. García-Fernández, G. Álvarez Narciandi, Y. Álvarez López, and F. Las-Heras Andrés, "Improvements in GPR-SAR imaging focusing and detection capabilities of UAV-mounted GPR systems," *ISPRS Journal of Photogrammetry and Remote Sensing*, vol. 189, pp. 128–142, 2022. [Online]. Available: https://www.sciencedirect.com/science/article/pii/S0924271622001113

[6] S. Kharkovsky, J. T. Case, M. A. Abou-Khousa, R. Zoughi, and F. L. Hepburn, "Millimeter-wave detection of localized anomalies in the space shuttle external fuel tank insulating foam," *IEEE Trans. Instrum. Meas.*, vol. 55, no. 4, pp. 1250–1257, Aug 2006.

[7] B. Larumbe, J. Laviada, A. Ibáñez-Loinaz, and J. Teniente, "Real-time imaging with frequency scanning array antenna for industrial inspection applications at W band," *Journal of Infrared, Millimeter, and Terahertz Waves*, vol. 39, no. 1, pp. 45–63, Jan 2018.

[8] J. Laviada, B. Wu, M. T. Ghasr, and R. Zoughi, "Nondestructive Evaluation of Microwave-Penetrable Pipes by Synthetic Aperture Imaging Enhanced by Full-Wave Field Propagation Model," *IEEE Transactions on Instrumentation and Measurement*, vol. 68, no. 4, pp. 1112–1119, 2019.

[9] H. Fernández Álvarez, G. Álvarez Narciandi, M. García-Fernández, J. Laviada, Y. Álvarez López, and F. Las-Heras Andrés, "A Portable Electromagnetic System Based on mm-Wave Radars and GNSS-RTK Solutions for 3D Scanning of Large Material Piles," *Sensors*, vol. 21, no. 3, 2021.

[10] N. K. Nikolova, "Microwave imaging for breast cancer," *IEEE Microwave Magazine*, vol. 12, no. 7, pp. 78–94, Dec 2011.

[11] M. T. Bevacqua, S. Di Meo, L. Crocco, T. Isernia, and M. Pasian, "Millimeter-waves breast cancer imaging via inverse scattering techniques," *IEEE Journal of Electromagnetics, RF and Microwaves in Medicine and Biology*, vol. 5, no. 3, pp. 246–253, 2021.

[12] M. Pastorino, *Microwave Imaging*. John Wiley & Sons, Inc., 2010.

[13] M. T. Ghasr, M. A. Abou-Khousa, S. Kharkovsky, R. Zoughi, and D. Pommerenke, "Portable real-time microwave camera at 24 GHz," *IEEE Trans. Antennas Propag.*, vol. 60, no. 2, pp. 1114–1125, Feb 2012.

[14] M. T. Ghasr, M. J. Horst, M. R. Dvorsky, and R. Zoughi, "Wideband Microwave Camera for Real-Time 3-D Imaging," *IEEE Trans. Antennas Propag.*, vol. 65, pp. 258 – 268, Jan 2017.

[15] R. Hussung, A. Keil, and F. Friederich, "Handheld millimeter wave imaging system based on a two-dimensional multistatic sparse array," in *2020 45th International Conference on Infrared, Millimeter, and Terahertz Waves (IRMMW-THz)*, 2020, pp. 1–2.

[16] J. Laviada, M. López-Portugués, A. Arboleya-Arboleya, and F. Las-Heras, "Multiview mm-wave imaging with augmented depth camera information," *IEEE Access*, vol. 6, pp. 16 869–16 877, 2018.

[17] G. Álvarez-Narciandi, M. López-Portugués, F. Las-Heras, and J. Laviada, "Freehand, Agile, and High-Resolution Imaging With Compact mm-Wave Radar," *IEEE Access*, vol. 7, pp. 95 516–95 526, 2019.

[18] G. Álvarez Narciandi, J. Laviada, and F. Las-Heras, "Freehand mm-Wave Imaging With a Compact MIMO Radar," *IEEE Transactions on Antennas and Propagation*, vol. 69, no. 2, pp. 1224–1229, 2021.

[19] I. Nasr, R. Jungmaier, A. Baheti, D. Noppeney, J. S. Bal, M. Wojnowski, E. Karagozler, H. Raja, J. Lien, I. Poupyrev, and S. Trotta, "A highly integrated 60 GHz 6-channel transceiver with antenna in package for smart sensing and short-range communications," *IEEE J. Solid-State Circuits*, vol. 51, no. 9, pp. 2066–2076, Sept 2016.

[20] Texas Instruments. (2023, Jan.) 60 GHz Radar-on-Chip. [Online]. Available: https://www.ti.com/tool/IWR6843AOPEVM

[21] Vayyar. (2023, Jan.) System on chip specification. [Online]. Available: http://vayyar.com/technology/

[22] X. Zhuge and A. G. Yarovoy, "Three-dimensional near-field MIMO array imaging using range migration techniques," *IEEE Trans. Image Process.*, vol. 21, no. 6, pp. 3026–3033, June 2012.

[23] J. W. Smith and M. Torlak, "Efficient 3-D Near-Field MIMO-SAR Imaging for Irregular Scanning Geometries," *IEEE Access*, vol. 10, pp. 10 283–10 294, 2022.

[24] S. Xing, S. Song, S. Quan, D. Sun, J. Wang, and Y. Li, "Near-Field 3D Sparse SAR Direct Imaging with Irregular Samples," *Remote Sensing*, vol. 14, no. 24, 2022. [Online]. Available: https://www.mdpi.com/2072-4292/14/24/6321

[25] H. Regmi, M. S. Saadat, S. Sur, and S. Nelakuditi, "SquiggleMilli: Approximating SAR Imaging on Mobile Millimeter-Wave Devices," *Proc. ACM Interact. Mob. Wearable Ubiquitous Technol.*, vol. 5, no. 3, sep 2021.

[26] Z. Hao, R. Wang, X. Dang, H. Yan, and J. Peng, "mmSight: A Robust Millimeter-Wave Near-Field SAR Imaging Algorithm," *Applied Sciences*, vol. 12, no. 23, 2022. [Online]. Available: https://www.mdpi.com/2076-3417/12/23/12085

[27] J. W. Smith, Y. Alimam, G. Vedula, and M. Torlak, "A Vision Transformer Approach for Efficient Near-Field SAR Super-Resolution under Array Perturbation," in *2022 IEEE Texas Symposium on Wireless and Microwave Circuits and Systems (WMCS)*, 2022, pp. 1–6.

[28] J. Laviada, G. Álvarez Narciandi, and F. Las-Heras, "Artifact Mitigation for High-Resolution Near-Field SAR Images by Means of Conditional

Generative Adversarial Networks," *IEEE Transactions on Instrumentation and Measurement*, vol. 71, pp. 1–11, 2022.
[29] C. Vasileiou, J. Smith, S. Thiagarajan, M. Nigh, Y. Makris, and M. Torlak, "Efficient CNN-Based Super Resolution Algorithms for Mmwave Mobile Radar Imaging," in *2022 IEEE International Conference on Image Processing (ICIP)*, 2022, pp. 3803–3807.
[30] P. T. Hien and I.-P. Hong, "Millimeter Wave SAR Imaging Denoising and Classification by Combining Image-to-Image Translation With ResNet," *IEEE Access*, vol. 11, pp. 70 203–70 215, 2023.
[31] J. M. Schellberg, H. Regmi, and S. Sur, "mmSight: Towards Robust Millimeter-Wave Imaging on Handheld Devices," in *2023 IEEE 24th International Symposium on a World of Wireless, Mobile and Multimedia Networks (WoWMoM)*, 2023, pp. 117–126.
[32] Q. Wen and S. Cao, "Quantitative Investigation of Imaging Quality vs. Radar Position Errors in Millimeter-wave SAR," in *2023 IEEE Radar Conference (RadarConf23)*, 2023, pp. 1–6.
[33] Z. Zhao, W. Tian, Y. Deng, C. Hu, and T. Zeng, "Calibration Method of Array Errors for Wideband MIMO Imaging Radar Based on Multiple Prominent Targets," *Remote Sensing*, vol. 13, no. 15, 2021. [Online]. Available: https://www.mdpi.com/2072-4292/13/15/2997
[34] G. Álvarez-Narciandi, J. Laviada, Y. Álvarez-López, and F. Las-Heras, "Portable Freehand System for Real-Time Antenna Diagnosis and Characterization," *IEEE Transactions on Antennas and Propagation*, vol. 68, no. 7, pp. 5636–5645, 2020.
[35] G. Álvarez Narciandi, J. Laviada, Y. Álvarez López, G. Ducournau, C. Luxey, C. Belem-Goncalves, F. Gianesello, N. Nachabe, C. D. Rio, and F. Las-Heras, "Freehand system for antenna diagnosis based on amplitude-only data," *IEEE Transactions on Antennas and Propagation*, vol. 69, no. 8, pp. 4988–4998, 2021.
[36] O. Li, J. He, K. Zeng, Z. Yu, X. Du, Y. Liang, G. Wang, Y. Chen, P. Zhu, W. Tong, D. Lister, and L. Ibbotson, "Integrated Sensing and Communication in 6G A Prototype of High Resolution THz Sensing on Portable Device," in *2021 Joint European Conference on Networks and Communications & 6G Summit (EuCNC/6G Summit)*, 2021, pp. 544–549.
[37] O. Li, J.He, K. Zeng, Z. Yu, X. Du, Z. Zhou, Y. Liang, G. Wang, Y. Chen, P. Zhu, W. Tong, D. Lister, and L. Ibbetson, "Integrated sensing and communication in 6G: a prototype of high resolution multichannel THz sensing on portable device," *EURASIP Journal on Wireless Communications and Networking*, no. 106, 2022.
[38] G. Álvarez Narciandi, J. Laviada, and F. Las-Heras, "Towards turning smartphones into mmWave scanners," *IEEE Access*, vol. 9, pp. 45 147–45 154, 2021.
[39] C. Cadena, L. Carlone, H. Carrillo, Y. Latif, D. Scaramuzza, J. Neira, I. Reid, and J. J. Leonard, "Past, Present, and Future of Simultaneous Localization and Mapping: Toward the Robust-Perception Age," *IEEE Transactions on Robotics*, vol. 32, no. 6, pp. 1309–1332, 2016.
[40] G. Álvarez Narciandi, J. Laviada, and F. Las-Heras, "Impact of the Number of Transmitting-Receiving Channels on the Quality of the Images Obtained by a Millimeter-Wave Freehand Imager," in *2022 16th European Conference on Antennas and Propagation (EuCAP)*, 2022, pp. 1–4.
[41] G. Álvarez-Narciandi, J. Laviada, and F. Las-Heras, "Freehand millimeter-wave imaging system based on a highly-integrated MIMO radar module," in *Passive and Active Millimeter-Wave Imaging XXV*, vol. 12111, International Society for Optics and Photonics. SPIE, 2022. [Online]. Available: https://doi.org/10.1117/12.2622638
[42] Intel RealSense. (2023, Jan.) Tracking camera t265. [Online]. Available: https://www.intelrealsense.com/tracking-camera-t265/
[43] OptiTrack. (2023, Jan.) Optitrack motion capture system. [Online]. Available: http://www.optitrack.com
[44] Y. Gao, M. T. Ghasr, and R. Zoughi, "Effects of and Compensation for Translational Position Error in Microwave Synthetic Aperture Radar Imaging Systems," *IEEE Transactions on Instrumentation and Measurement*, vol. 69, no. 4, pp. 1205–1212, 2020.
[45] Z. Wang, E. Simoncelli, and A. Bovik, "Multiscale structural similarity for image quality assessment," in *The Thrity-Seventh Asilomar Conference on Signals, Systems N& Computers, 2003*, vol. 2, 2003, pp. 1398–1402 Vol.2.